Thickness dependent vibrational and electronic properties of MnO(100) thin films grown on Pt(111)

Steffen Sachert, Sebastian Polzin, Krassimir Kostov,* and Wolf Widdra†
Institute of Physics, Martin-Luther-Universität Halle-Wittenberg, Halle, Germany
(Received 23 March 2010; published 18 May 2010)

MnO films have been grown by reactive metal deposition in an O_2 atmosphere on Pt(111). The vibrational and electronic excitations between 50 meV and 7 eV have been investigated by high-resolution electron energy loss spectroscopy as function of layer thickness up to 17 ML. The vibrational spectrum of the MnO monolayer is characterized by a strong and narrow phonon at 368 cm^{-1}. For coverages above the monolayer the oxide film is characterized by a Wallis mode and a Fuchs-Kliewer phonon (382 and 547 cm^{-1}). Whereas the Wallis mode has constant intensity and frequency, the Fuchs-Kliewer phonon intensity increases and its frequency decreases with coverage as predicted by dielectric theory. Mild annealing (<850 K) of MnO films improves the long-range ordering while higher temperatures causes dewetting and cluster formation. For thin films between 4 and 10 monolayers the losses due to electronic transitions within the Mn 3*d* states have been studied. Six transitions could be identified which indicate for thick films an electronic structure similar to the one found for MnO(100) single crystal surface. Additionally, surface related *d-d* transitions have been identified.

DOI: 10.1103/PhysRevB.81.195424 PACS number(s): 68.47.Gh, 68.35.Ja, 63.22.Np

I. INTRODUCTION

The physical and chemical properties of 3*d* transition-metal oxides cover a broad spectrum depending on the filling of the 3*d* states.[1] Particularly manganese oxides are technologically interesting as electrode material, for magnetic applications, and in heterogeneous catalysis.[2–4] Furthermore as ultrathin films or nanoparticles manganese oxides exhibit unusual magnetic and electronic properties.[5–8]

The bulk properties of the antiferromagnetic [Néel temperature, T_N=118 K (Ref. 9)] MnO which crystallizes in the rocksalt structure with a lattice constant of a_{MnO} =0.444 nm (Ref. 10) and exhibits a band gap of 3.6–4.3 eV (Ref. 11 and references therein) are well established. Its electronic structure is characterized by a Mn^{+2} $3d^5$ high-spin configuration with a behavior between a charge transfer and a Mott-Hubbard insulator.[12–14] The dielectric properties[15–21] and electronic excitations such as the *d-d* transitions[11,13,22,23] have been investigated. Early work on the vibrational properties shows that the transversal-optical (TO) phonon is located at the Γ point at about 265 cm^{-1}.[16,17,19,24] Below the phase-transition temperature of 118 K, a splitting of the TO phonon of approximately 30 cm^{-1} has been observed due to the magnetic ordering.[18,20,25,26]

For structurally well characterized ultrathin films of MnO there is much less known. Several groups reported successful growth on top of single-crystal metals as Ag(100), Rh(100), Pd(100), and Pt(111).[27–38] Mainly growth of MnO(100)-oriented films had been found. On the other hand for the growth on Pd(100) a variety of different manganese oxide monolayer (ML) structures have been characterized and there phonon spectra reported.[37] For a MnO(100)-like monolayer on Pd(100) an dipole-active phonon at 350–360 cm^{-1} has been found which is close to 368 cm^{-1} observed for the MnO(100) monolayer on Pt(111).[33] MnO(100) films on Pd(100) with a thickness of 20–30 ML on the other hand are characterized by a phonon at 524 cm^{-1}.[34,35]

However a systematic study of the evolution of the vibrational and electronic structure with increasing thin film thickness is still missing. This is the goal of the present work. We report on a continuous shift of the dominant Fuchs-Kliewer (FK) phonon with layer thickness which is discussed in terms of the confinement of the bulk TO phonon to the MnO(100) thin film. In addition, we report on layer-resolved *d-d* excitations which allow for a detailed characterization of transport-related electronic properties. These ultrathin film data for a highly correlated transition-metal oxide system might stimulate further theoretical studies. Complementary investigations of the layer-resolved electronic structure by scanning tunneling spectroscopy are in preparation.

II. EXPERIMENT

The experiments have been performed in a two chamber ultrahigh vacuum (UHV) system. The base pressure was below 1×10^{-10} mbar. One chamber is equipped with standard surface science methods for sample cleaning (Ar^+ sputtering, heating) and characterization (low-energy electron diffraction, LEED) and with thermal-desorption spectroscopy (TPD) facilities. The second UHV chamber houses a spectrometer for high-resolution electron energy loss spectroscopy (HREELS; Delta 05, Specs, Germany). The system is described in more details elsewhere.[39,40] The Pt(111) surface was cleaned by repeated cycles of Ar^+ sputtering at room temperature, subsequent annealing cycles in oxygen (1100 K) and final flashing to 1300 K. Cleanness was checked by LEED and HREELS, no loss features were detected besides spurious amounts of CO on Pt(111). Before Mn deposition the sample was annealed to 600 K to desorb traces of adsorbate as, e.g., CO and H_2O. Thin films of MnO were grown on Pt(111) at a temperature of 375 K by deposition of Mn in O_2 atmosphere of 5×10^{-8} mbar. These values were chosen with reference to earlier work.[27,33] As described previously CO titration experiments were used in the submonolayer re-

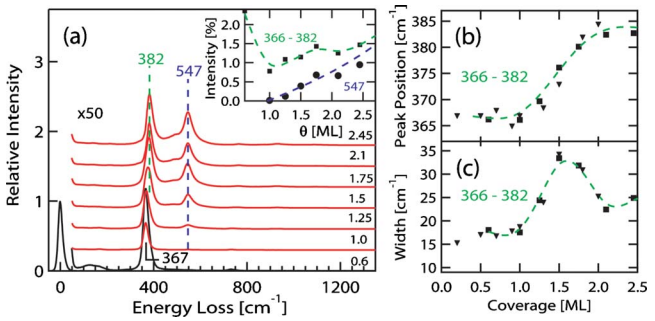

FIG. 1. (Color online) (a) HREEL spectra of MnO grown on Pt(111) with coverages between 0.6 and 2.5 ML. The coverages are indicated at the right of Fig. 1(a). Inset: relative intensities of the two main features. (b) Energy of the phonon between 366 and 382 cm^{-1} as function of film thickness. (c) Deconvoluted width of the phonon between 366 and 382 cm^{-1} as function of film thickness. Squares and triangles in (b) and (c) indicate two different growth series.

gime to estimate the Mn-deposition rate.[33] The Mn-deposition rate was monitored and controlled by the flux of Mn ions present in the beam. The structural ordering has been improved by post annealing the sample in UHV at 650 K for 20 s after every growth step. If not stated otherwise all HREEL spectra were recorded at 80 K with an electron energy of 4 eV. The experiments have been performed in specular reflecting geometry with a total 120° scattering angle.

III. RESULTS AND DISCUSSION

A. Growth

Figure 1(a) shows the evolution of the vibrational spectra of MnO on Pt(111) for coverages between 0.6 and 2.5 ML. Two main features are visible. One peak at about 367 cm^{-1} which shifts with increasing coverage to higher energies and one peak which becomes visible at coverages above 1 ML. In the inset of Fig. 1(a) the relative intensities of these two peaks are shown. While for the intensity of the phonon at about 367 cm^{-1} only a small increase between 1 and 2 ML is observed, the phonon at 547 cm^{-1} shows a clear approximately linear increase in intensity with increasing coverage. The energy and width of the main loss are shown in Figs. 1(b) and 1(c), respectively. The phonon energy of this energy loss has a constant value of 367 cm^{-1} below 1 ML. Between 1 and 2 ML the energy increases monotonously to 382 cm^{-1} and stays approximately constant at this value above 2 ML. The width of this phonon broadens between 1 and 2 ML, and shows a maximum at 1.5 ML. These properties indicate that the peak is composed of two phonons, one at 367 cm^{-1} belonging to the first monolayer and one at 382 cm^{-1} belonging to the second monolayer. The intensities of the two phonons depend on the areas with local thickness of 1 and 2 ML, respectively. The coverage dependence of the width and energy of the resulting energy loss indicate a layerlike growth at least up to 2 ML.

Figure 2 shows HREEL spectra for MnO films of coverages of 0.9 (Ref. 33) and 2.3 ML which have been prepared with different oxygen isotopes (^{16}O or ^{18}O). The observed phonon frequencies for the Mn ^{18}O layers are shifted down by 4% related to the otherwise similarly prepared Mn ^{16}O films. This down shift is related to the different oxygen masses of the vibrating entities. A value of 4% is expected for a phonon mode in which the oxygen sublattice vibrates against the manganese sublattice. In contrast to thicker MnO films (discussed below) all vibrational feature show narrow line shapes. Especially the well-annealed monolayer can exhibit a phonon linewidth below 9 cm^{-1} when correcting for the instrumental resolution.

Figure 3(a) summarizes the phonon spectra for coverages up to 17 ML. The phonon energies and intensities are presented in Figs. 3(b) and 3(c), respectively. Above 2 ML neither the energy nor the intensity of the phonon at 382 cm^{-1} is affected by the film thickness. Above 8 ML the energy loss is hardly visible since it is covered by the strong phonon at about 540 cm^{-1}. The phonon at 382 cm^{-1} has been interpreted as Wallis mode which is a displacement pattern where the first-layer O atoms vibrate along the surface normal.[41,42]

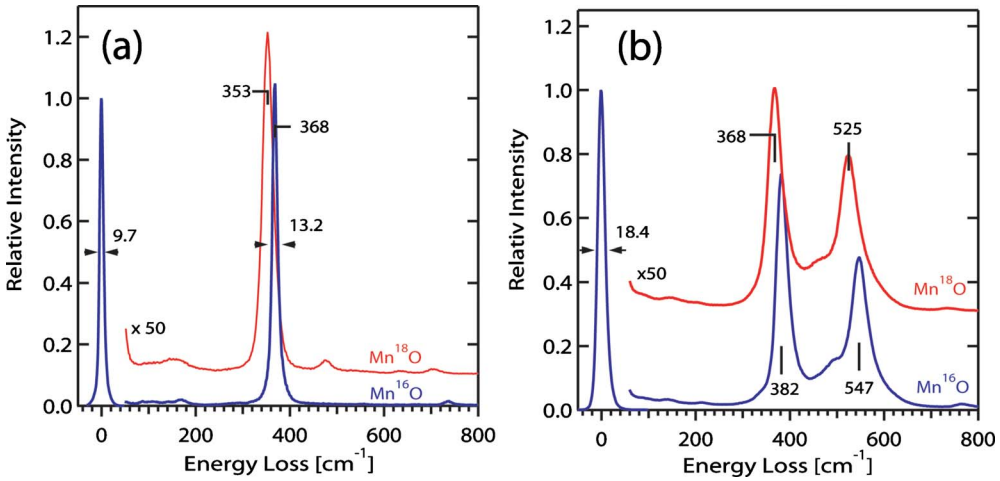

FIG. 2. (Color online) HREEL spectra of Mn ^{16}O (blue) and Mn ^{18}O (red) grown on Pt(111) with coverages of (a) 0.9 and (b) 2.3 ML. (a) Adapted from (Ref. 33).

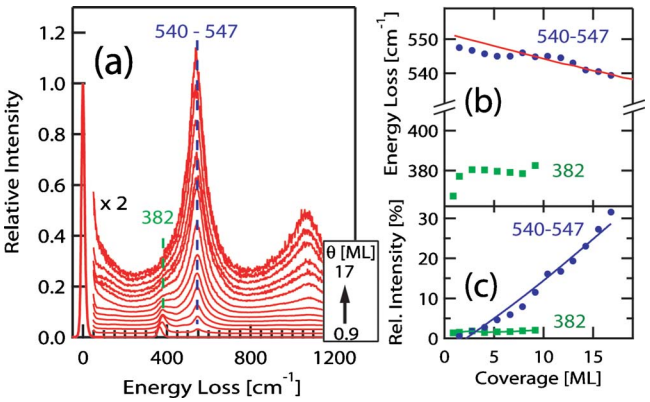

FIG. 3. (Color online) (a) HREEL spectra of MnO(100)-like thin films grown on Pt(111) with thicknesses between 0.9 and 17 ML. The coverages are: 0.9, 1.5, 2.8, 4.1, 5.3, 6.6, 7.9, 9.2, 10.4, 11.7, 13.0, 14.2, 15.5, and 16.8 ML (±10%). (b) Energies of the two main phonons as function of film thickness (dots and squares) and calculated thickness dependence of the Fuchs-Kliewer phonon (solid line). (c) Intensity of the two main phonons as function of film thickness. In Figs. 2(b) and 2(c) the loss at about 382 cm^{-1} is indicated by green squares and the loss between 547 and 546 cm^{-1} by blue solid circles.

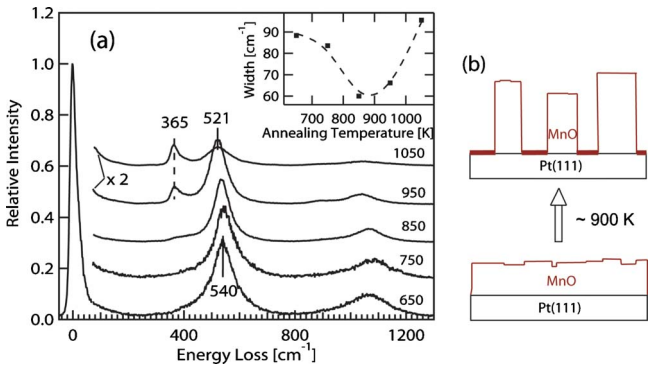

FIG. 4. (Color online) (a) HREEL spectra of 17-ML-thick MnO(100) film grown on Pt(111) as function of subsequent annealing. Annealing temperatures are indicated on the right (annealing for 20 s). (b) Schematic of the restructuring of the MnO film due to annealing above 900 K.

Due to its local character the constant energy and intensity indicates that the Mn-O bonding in the outermost 1–2 layers is rather similar for all thicknesses beyond 2 ML. A similar Wallis mode was observed for MgO thin films on Ag(100) which shows an analogous coverage dependence as observed in our experiments.[43] The second phonon mode (≈540 cm^{-1}) has been identified as FK phonon.[44] The FK is a macroscopic surface phonon polariton which represents the dielectric response of the MnO film.

Langell *et al.*[45] observed this mode for single crystals at 572 and 525 cm^{-1} depending on the sample preparation. Whereas the value at 572 cm^{-1} is unexpectedly located outsides the gap between the transversal optical mode [ω_{TO} =262 cm^{-1} (Ref. 16)] and the longitudinal optical mode [ω_{LO}=552 cm^{-1} (Ref. 16)] of bulk MnO, the value of 525 cm^{-1} is well located in the expected phonon gap. The latter also corresponds well to the observed HREEL spectra of thin MnO films grown on Pd(100) which show a single narrow phonon at 524 cm^{-1}.[34,46] A detailed comparison with the theoretical expected coverage dependence of the FK will be given below.

B. Annealing

Annealing experiments have been performed to improve the long-range order of the film and to identify thermal decomposition processes within the film. Figure 4(a) shows vibrational spectra for a 17-ML-thick MnO film on Pt(111) upon sequential annealing in UHV. The lowest spectrum is the same as the upper spectrum in Fig. 3(a). In all spectra the FK at about 540 cm^{-1} is visible. Whereas up to 850 K only minor changes occur, annealing to 950 K leads to a significant down shift of the FK to 521 cm^{-1}. Additionally after annealing at 950 and 1050 K an energy loss at 365 cm^{-1} is observed. The width of the FK as function of annealing temperature is shown in the inset of Fig. 4(a). One can clearly distinguish a decrease in the width up to annealing temperatures of 850 K which is explained by long range ordering of the MnO film. Note that the minimum width of about 60 cm^{-1} is significantly wider for the 17-ML film as compared to the 2-ML film discussed before. Upon further annealing beyond 850 K a broadening of the phonon can be observed which is accompanied by a sample charging effect resulting in a decreasing intensity of the elastic peak with time. For that reason the relative intensities in Fig. 4(a) are hardly comparable. All these observations can be explained by an ordering of the MnO film up to annealing temperatures of 850 K and a restructuring of the MnO film into larger islands and a remaining MnO monolayer which is recognized by the phonon peak at 365 cm^{-1} above this temperature.[33] A schematic representation is given in Fig. 4(b). The larger islands result in a FK phonon at 521 cm^{-1}. Height variations in the islands explain the slightly increased width of this phonon. In LEED images the Pt(111)-(1×1) substrate and the characteristic (19×1) MnO(100) monolayer diffraction peaks became visible due to annealing (not shown here) which is a further independent evidence for a dewetting of the MnO film. However, a total dewetting which would expose a bare or oxygen-covered substrate can be excluded on the basis of the HREEL spectra. For the bare Pt(111) surface the adsorption of CO from the residual gas is inevitable which is characterized by a strong energy loss at 2100 cm^{-1} due to the internal stretching mode of on top adsorbed CO.[47] Since this vibration is absent an upper limit of 0.1 ML for areas of bare Pt(111) can be given. On the other hand also no desorption of O has been observed in TPD during annealing. By the same observation a segregation of Mn into the platinum substrate can be widely excluded as this would cause an increase in the oxygen amount in the manganese oxide which would be visible in the energy loss spectra. Consequently the MnO film restructures into thicker MnO(100) cluster on a MnO(100)-like monolayer. Since the observed charging effects disable a comparison of the relative intensity an estimation of the cluster height is difficult. On the other hand a charging of the sample is a hint for high MnO clusters which can be explained by the isolat-

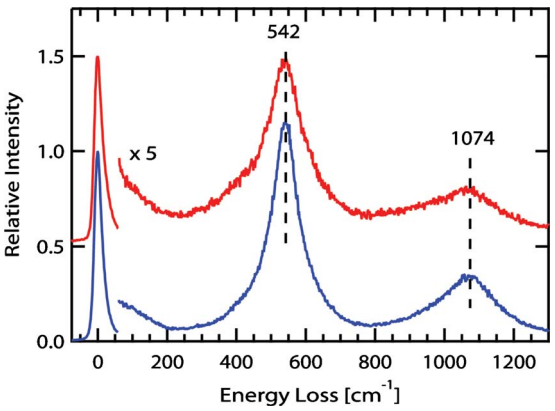

FIG. 5. (Color online) HREEL spectra of a 10-ML-thick MnO film on Pt(111) measured at 85 (lower blue) and 300 K (upper red).

ing behavior of these cluster (band-gap MnO 3.6–4.3, Ref. 48 and citations therein). However if we assume an area of 2/3 of the dewetted first monolayer and 1/3 cluster for an initial coverage of 17 ML, an average cluster height of 40–50 ML follows. The observed energy of the FK (521 cm^{-1}) is than in agreement with theoretical values (see below) and experimental observed values by Allegretti *et al.*[34] and Langell *et al.*[45] for a 30-ML-thick MnO film on Pd(100) and for a MnO(100) single crystal, respectively. The transformation of the MnO thin film into MnO clusters occurs in a wider temperature range which depends on the oxide film thickness (not shown here).

C. Dielectric response

Figure 5 shows vibrational spectra of 10 ML MnO on Pt(111) taken below and above the bulk Néel temperature. The paramagnetic antiferromagnetic transition results in a slight distortion of the ideal rock salt structure. The former cubic structure (α=90°) transforms into a rhomboidal structure [α=90.62° at 4.8 K (Ref. 49)]. Beside the structural change the phase transition influences also the vibrational properties as can be seen in a splitting of the transversal optical phonon (ω_{TO}) of about 30 cm^{-1} due to the spin ordering as observed for a MnO single crystal.[18,20] One would expect to observe a related splitting of the FK, respectively. At the given experimental resolution of about 27 cm^{-1} a splitting of 30 cm^{-1} would be visible as a broadening of the FK. However a broadening of the FK at 85 K relative to the width of the phonon at 300 K is not visible in Fig. 5. At both temperatures the FK phonon is rather broad with a slightly higher width at RT. Therefore the data in Fig. 5 do not allow to conclude on the magnetic ordering of the film. On the other hand the absence of a strong temperature dependence enables one to use RT material constants to calculate the expected coverage dependence of the FK. For a single crystal or a thick film the energy of the FK can easily be estimated by[50]

$$\omega_{FK} = \sqrt{\frac{\varepsilon_0 + 1}{\varepsilon_\infty + 1}}\omega_{TO}, \tag{1}$$

where ε_∞ is the high-frequency dielectric constant, ε_0 the static dielectric constant, and ω_{TO} the energy of the zone-center transverse optical phonon. These values vary slightly in literature.[15–21] In the following we use ε_∞=4.85, ε_0=20.6, and ω_{TO}=269 cm^{-1}.[20] Equation (1) leads to an energy of the FK of 517 cm^{-1} which is in good agreement with the experimentally observed value for thick films.

As has been discussed for MgO, LiBr, and NiO thin films, the expected energy of the FK is thickness dependent. It can be calculated by taking the dielectric response into account. The spectral function of inelastic electron scattering can be described by a classical energy loss probability (P_{cl}).[51–55] The loss probability describes for a given acceptance area D of the HREELS spectrometer, a given electron velocity $\vec{v}$ of the incoming electrons, and a given film thickness d the spectral response

$$P_{cl}(\omega,d) = \frac{4e^2}{\pi^2\hbar v_\perp}\int_D \underbrace{\frac{q_\parallel \cdot v_\perp^3}{[(\omega - \vec{q}_\parallel\vec{v}_\parallel)^2 + (q_\parallel v_\perp)^2]^2}}_{F} \times \underbrace{\mathrm{Im}\frac{-1}{\xi_0(\vec{q}_\parallel,\omega,d)+1}}_{I} d^2q_\parallel. \tag{2}$$

Here $\vec{q}_\parallel$ is the momentum transfer parallel to the surface, and $v_\parallel$ and $v_\perp$ are the electron-velocity components parallel and perpendicular to the surface. $\xi_0(\vec{q}_\parallel,\omega,d)$ is the effective dielectric function of the thin-film system. The first part of the integrand in Eq. (2) F is a kinematics prefactor that describes the spatial behavior of the HREELS cross section.[54] Electrons which have undergone an energy loss experience also a small momentum transfer and are therefore scattered slightly out of the specular direction. For example, for a given energy loss of about 550 cm^{-1} the maximum of F can be observed at $q_\parallel$=0.08 nm^{-1}. The second part I describes the energy-loss function due to the response of the system.[54] The effective dielectric function for a two-layer system can be described as[55]

$$\xi_0(\vec{q}_\parallel,\omega,d) = \epsilon\cdot\coth(q_\parallel d) - \frac{[\epsilon/\sinh(q_\parallel d)]^2}{\epsilon\cdot\coth(q_\parallel d) + \xi_1(\vec{q}_\parallel,\omega)}, \tag{3}$$

where the ϵ and d are the dielectric function and the thickness of the first layer. ξ_1 is the dielectric function of the second layer which is the Pt(111) substrate here. In case of MnO on Pt(111), ϵ is the dielectric function of MnO which can be written as

$$\epsilon(\omega) = \varepsilon_\infty + \frac{(\varepsilon_0 - \varepsilon_\infty)\omega_{TO}^2}{\omega_{TO}^2 - \omega^2 - i\gamma\omega\omega_{TO}}, \tag{4}$$

where γ is a damping constant. The dielectric function of platinum can be approximated by a simple Drude Ansatz $\xi_1(\omega) = -\omega_P^2/(\omega^2 + i\gamma_P\omega\omega_P)$. Here ω_P is the frequency of the surface plasmon ω_P=23 eV (Refs. 56 and 57) and γ_P the corresponding damping (γ_P=0.1).

Figure 6(a) shows a comparison between the HREEL spectra of 10-ML MnO on Pt(111) (black line) and the calculated spectral response for the thin film of the same thickness using $q_\parallel$=0.08 nm^{-1} (red solid line). The oxide damping constant γ has been varied to fit the experimental width

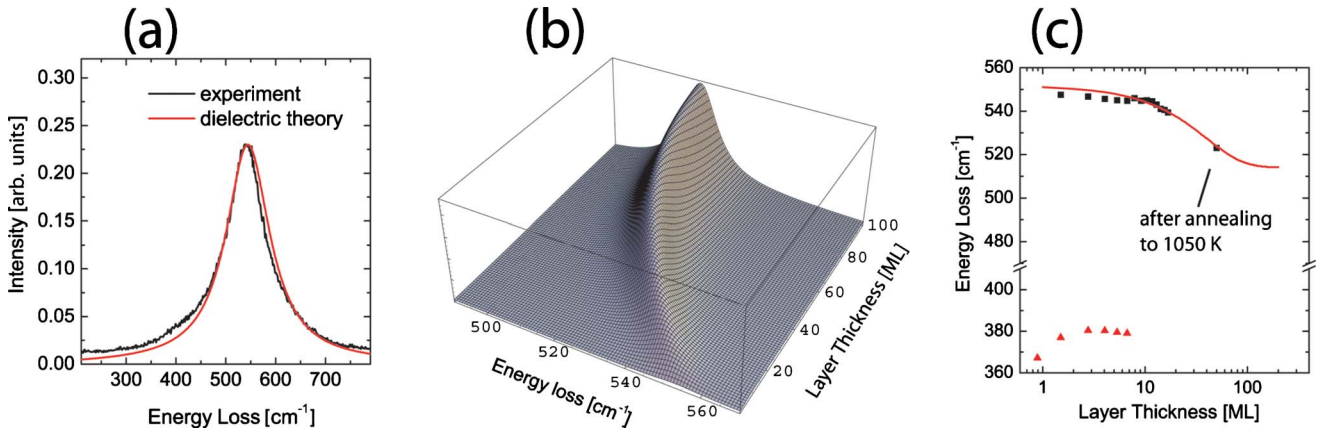

FIG. 6. (Color online) (a) Comparison of experimental HREEL spectra (black) and result of function I (red) for 10-ML MnO on Pt(111). For the calculation of I $\gamma=0.4$ and $q_{\parallel}=0.08$ nm^{-1} has been used. (b) Results of function I as function of MnO film thickness (the term $q^{*}d$ has been transferred into film thickness by $0.08^{*}d$ and $d=N\times a_{\mathrm{MnO}(100)}=N^{*}0.222$ nm with N as the number of layers) For a better visibility $\gamma=0.05$ has been used. (c) Comparison between calculated (straight line) and experimental (squares) estimated energy of the FK as function of film thickness, additionally the frequencies of the Wallis mode (triangles) are shown.

and has been estimated to be 0.4. The value is significant higher than the value observed for a MnO single crystal ($\gamma=0.05$ [Ref. 20)]. The origin of this broadening is not understood yet although some contribution from inelastic phonon scattering at the interface are expected.

The development of the spectral response with film thickness is shown in Fig. 6(b). To emphasis the phonon shift a $\gamma=0.05$ has been chosen for displaying the results. The calculation exhibits an intensity increase and redshift of the FK with increasing film thickness. The calculated redshift is compared to the experimental data in Fig. 6(c) as solid line and as square markers, respectively. For the MnO films with thickness over 8 ML the theory fits well with experiments. For thinner films there is a small deviation of the experimental data which might be caused by the macroscopic and continuous nature of the dielectric theory or by thin-film modifications of the bulk-derived constants due to structural relaxation at the interface.

D. Electronic structure

In Fig. 7 the loss spectra in the region of the electronic Mn d-d transitions are shown for the clean Pt(111) surface and for a MnO monolayer on Pt(111). The spectrum of bare Pt(111) shows a broad energy loss at about 0.6 eV which is attributed to a known interband transition of bulk platinum.[56] In addition a narrow loss at 0.25 eV is visible due to spurious amounts of adsorbed CO from residual gas.[58] Its width indicates the instrumental resolution (about 10 meV). Upon deposition of 0.9-ML MnO an additional energy loss structure appears in the range between 1.5 and 3.0 eV. Since the spectrum is still dominated by the Pt interband transition the difference spectrum after subtraction of the bare Pt(111) spectrum is shown in Fig. 7 (lowest spectrum). Similarly spectra for other MnO film thicknesses are presented in Fig. 8 after subtraction of a smooth background.

The EEL spectra undergo dramatic changes with increasing film thickness between 0.9 and 10 ML (Fig. 8 from bottom to top). In contrast to the broad spectral structure at 0.9 ML, narrow losses appear starting from the second and third MnO monolayers. As shown by the fitted curves in Fig. 8 six distinct d-d transitions with high intensity can be resolved in the energy range between 2 and 4 eV at 2.11, 2.55, 2.90, 3.21, 3.41, and 3.81 eV. Additionally there are broader structures at 4.61 and 5.18 eV and furthermore, the 10-ML spectrum can only be fitted successfully by allowing a peak at about 3.55 as indicated in Fig. 8. By comparison with previous studies[11,13,22,23] on MnO single crystals the resolved energy losses can be assigned to distinct d-d band transitions of the Mn^{2+} ions within MnO (Table I). It should be noted that all possible d-d transitions for MnO between 2 and 5 eV have been resolved here and that the resolution is improved by 1 order of magnitude compared to previous measurements using single crystals.[22] The good general agreement of the EELS data for MnO layers above 4 ML with those of a MnO(100) single crystal shows that the ultrathin films grown on Pt(111) have indeed clear MnO(100) character. In contrast the films in the thickness range of 1–4 ML show a different

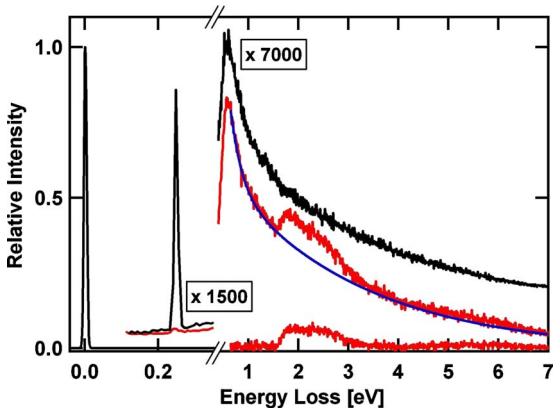

FIG. 7. (Color online) EEL spectra for bare and 0.9-ML MnO covered Pt(111). From top to bottom: Pt(111), 0.9-ML MnO on Pt(111), background (blue solid line) accounting for the Pt(111) substrate, and difference spectrum. Spectra have been recorded in specular direction with a primary electron energy of 36 eV.

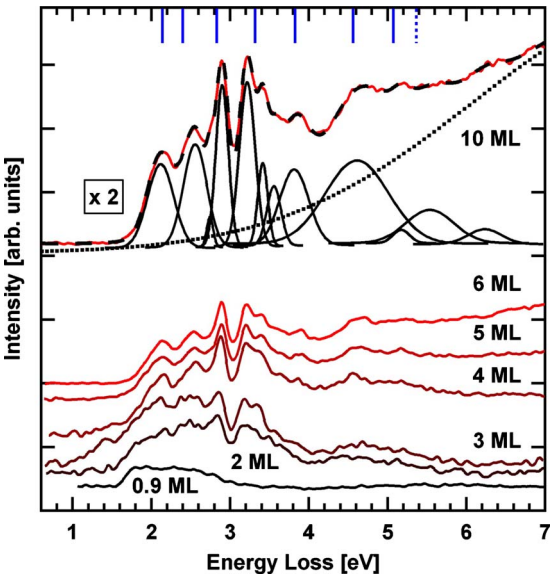

FIG. 8. (Color online) EEL spectra for MnO(100) film thickness (from bottom to top) of 0.9, 2, 3, 4, 5, 6, and 10 ML on Pt(111). The dashed line corresponds to a Gaussian multipeak fit for the 10-ML-thick film on top of a smooth background (dotted line). The fit consists of the several single peaks shown under the spectrum for the 10 ML. The markers at the top axes (blue) show the transitions observed for a MnO(100) single crystal (Ref. 22).

and less-pronounced peak structure. Especially the peak at about 3.4 eV shifts down below 4 ML and gains relative intensity. For the ultrathin films the *d-d* excitations of Mn ions at the inner and outer interface where a local C_{4v} symmetry is expected contribute stronger to the signal. Otherwise the spectra are dominated by Mn^{2+} ions located octahedrally between six O^{2-} ions (local O_h symmetry). At ultrathin films the excitations due to different symmetries overlap significantly. However, interface-related *d-d* excitations are identifiable at 1.85, 2.85, 3.18, and 3.34 eV.

The primary electron energy for the data of Fig. 8 has been chosen to 36 eV which corresponds to an observed oxygen $2p \rightarrow 3p$ resonance for the MnO single crystal.[11] However this resonant behavior could not be observed for the system MnO/Pt(111) here.

IV. CONCLUSION

The thickness dependent vibrational and electronic properties of MnO grown on Pt(111) have been investigated. The vibrational spectra are dominated by the Wallis mode at about 368 cm^{-1} and the Fuchs-Kliewer phonon. With increasing film thickness the Wallis mode is constant in energy and intensity. In contrast the FK shows a redshift with thickness and increases in intensity. The thickness dependence of the energy of the FK has been compared to dielectric theory and shows a good agreement for coverages above 8 ML. The long-range ordering of the MnO films can be improved by postannealing. However, at temperatures above 950 K a dewetting and MnO cluster formation takes place. The electronic excitations as determined by EEL spectra for an energy range up to 7 eV reveal that the electronic structure for film thickness above 4 ML is comparable to that of single crystals. The observed transitions could be attributed to *d-d* excitations in MnO. Only below 4-ML additional surface and interface excitations have been observed which are explained by the reduced surface symmetry.

TABLE I. Possible final states for a *d-d* excitation from the $^6A_{1g}$ ground state in the MnO. Reference Fromme (Refs. 11 and 22) is measured by electron energy loss spectroscopy and the results from Refs. 13 and 23 have been calculated. All the energies are given in eV.

d-d transition	Refs. 11 and 22	Ref. 13	Ref. 23	This work
$^4T_{1g}(^4G)$	2.13	2.31	2.01	2.11
$^4T_{2g}(^4G)$	2.4	2.93	2.56	2.55
$^4A_{1g}(^4G)$			2.94	2.90
$^4E_g(^4G)$	2.82	3.34	2.95	3.21
$^4T_{2g}(^4D)$	3.31	3.72	3.5	3.41
$^4E_g(^4D)$	3.82	3.96	3.69	3.81
$^4T_{1g}(^4P)$	4.57	4.43	4.2	4.61
$^4A_{2g}(^4F)$	5.08	5.35		5.18
$^4T_{1g}(^4F)$	5.38	5.58		
$^4T_{2g}(^4F)$		6.01		

ACKNOWLEDGMENTS

Financial support by the Deutsche Forschungsgemeinschaft (DFG) Sonderforschungsbereich SFB 762 "Functional Oxidic Interfaces" is gratefully acknowledged.

*Permanent address: Institute of General and Inorganic Chemistry, Bulgarian Academy of Sciences, Sofia, Bulgaria.
†Corresponding author; wolf.widdra@physik.uni-halle.de

[1] V. E. Henrich and P. A. Cox, *The Surface Science of Metal Oxides* (Cambridge University Press, Cambridge, 1996).
[2] A. R. Armstrong and P. G. Bruce, Nature (London) **381**, 499 (1996).
[3] M. Baldi, E. Finocchio, C. Pistarino, and G. Busca, Appl. Catal., B **173**, 61 (1998).
[4] M. J. Han, T. Ozaki, and J. J. Yu, J. Chem. Phys. **123**, 034306 (2005).
[5] W. S. Seo, H. H. Jo, K. Lee, B. Kim, S. J. Oh, and J. T. Park, Angew. Chem. Int. Ed. **43**, 1115 (2004).
[6] J. Park, E. A. Kang, C. J. Bae, J. G. Park, H. J. Noh, J. Y. Kim, J. H. Park, H. M. Park, and T. Hyeon, J. Phys. Chem. B **108**, 13594 (2004).
[7] I. Djerdj, D. Arcon, Z. Jaglicic, and M. Niederberger, J. Phys. Chem. C **111**, 3614 (2007).

[8] W. Neubeck, C. Vettier, V. Fernandez, F. de Bergevin, and C. Giles, J. Appl. Phys. **85**, 4847 (1999).
[9] A. L. Goodwin, M. G. Tucker, M. T. Dove, and D. A. Keen, Phys. Rev. Lett. **96**, 047209 (2006).
[10] W. B. Pearson, *Handbook of Lattice Spacings and Structures of Metals and Alloys* (Pergamon, New York, 1958).
[11] B. Fromme, U. Brunokowski, and E. Kisker, Phys. Rev. B **58**, 9783 (1998).
[12] A. Fujimori, N. Kimizuka, T. Akahane, T. Chiba, S. Kimura, F. Minami, K. Siratori, M. Taniguchi, S. Ogawa, and S. Suga, Phys. Rev. B **42**, 7580 (1990).
[13] J. van Elp, R. H. Potze, H. Eskes, R. Berger, and G. A. Sawatzky, Phys. Rev. B **44**, 1530 (1991).
[14] S. Hüfner, Adv. Phys. **43**, 183 (1994).
[15] T. P. Sharma, Solid State Commun. **20**, 1137 (1976).
[16] J. N. Plendl, L. C. Mansur, S. S. Mitra, and I. F. Chang, Solid State Commun. **7**, 109 (1969).
[17] B. C. Haywood and M. F. Collins, J. Phys. C **4**, 1299 (1971).
[18] E. M. L Chung, D. M. Paul, G. Balakrishnan, M. R. Lees, A. Ivanov, and M. Yethiraj, Phys. Rev. B **68**, 140406(R) (2003).
[19] T. B. Kinney and M. Okeeffe, Solid State Commun. **7**, 977 (1969).
[20] T. Rudolf, C. Kant, F. Mayr, and A. Loidl, Phys. Rev. B **77**, 024421 (2008).
[21] S. Mochizuki, J. Phys.: Condens. Matter **1**, 10351 (1989).
[22] B. Fromme, *d-d Excitations in Transition-Metal Oxides: A Spin-Polarized Electron Energy-Loss Spectroscopy (SPEELS) Study* (Springer-Verlag, Berlin, 2001).
[23] L. E. Orgel, J. Chem. Phys. **23**, 1004 (1955).
[24] S. K. Agarwal, Solid State Commun. **29**, 197 (1979).
[25] S. Massidda, M. Posternak, A. Baldereschi, and R. Resta, Phys. Rev. Lett. **82**, 430 (1999).
[26] W. D. Luo, P. H. Zhang, and M. L. Cohen, Solid State Commun. **142**, 504 (2007).
[27] F. Müller, R. de Masi, D. Reinicke, P. Steiner, S. Hüfner, and K. Stowe, Surf. Sci. **520**, 158 (2002).
[28] E. A. Soares, R. Paniago, V. E. de Carvalho, E. L. Lopes, G. J. P. Abreu, and H.-D. Pfannes, Phys. Rev. B **73**, 035419 (2006).
[29] M. Nagel, I. Biswas, H. Peisert, and T. Chasse, Surf. Sci. **601**, 4484 (2007).
[30] A. Chassé, C. Langheinrich, F. Müller, and S. Hüfner, Surf. Sci. **602**, 597 (2008).
[31] G. A. Rizzi, R. Zanoni, S. Di Siro, L. Perriello, and G. Granozzi, Surf. Sci. **462**, 187 (2000).
[32] G. A. Rizzi, M. Petukhov, M. Sambi, R. Zanoni, L. Perriello, and G. Granozzi, Surf. Sci. **482-485**, 1474 (2001).
[33] C. Hagendorf, S. Sachert, B. Bochmann, K. Kostov, and W. Widdra, Phys. Rev. B **77**, 075406 (2008).
[34] F. Allegretti *et al.*, Phys. Rev. B **75**, 224120 (2007).
[35] V. Bayer, R. Podloucky, C. Franchini, F. Allegretti, B. Xu, G. Parteder, M. G. Ramsey, S. Surnev, and F. P. Netzer, Phys. Rev. B **76**, 165428 (2007).
[36] F. Li, G. Parteder, F. Allegretti, C. Franchini, R. Podloucky, S. Surnev, and F. P. Netzer, J. Phys.: Condens. Matter **21**, 134008 (2009).
[37] C. Franchini, R. Podloucky, F. Allegretti, F. Li, G. Parteder, S. Surnev, and F. P. Netzer, Phys. Rev. B **79**, 035420 (2009).
[38] H. Nishimura, T. Tashiro, T. Fujitani, and J. Nakamura, J. Vac. Sci. Technol. A **18**, 1460 (2000).
[39] K. L. Kostov, M. Gsell, P. Jakob, T. Moritz, W. Widdra, and D. Menzel, Surf. Sci. **394**, L138 (1997).
[40] T. Moritz, D. Menzel, and W. Widdra, Surf. Sci. **427-428**, 64 (1999).
[41] R. F. Wallis, Phys. Rev. **105**, 540 (1957).
[42] R. F. Wallis, Phys. Rev. **116**, 302 (1959).
[43] L. Savio, E. Celasco, L. Vattuone, M. Rocca, and P. Senet, Phys. Rev. B **67**, 075420 (2003).
[44] R. Fuchs and K. L. Kliewer, Phys. Rev. **140**, A2076 (1965).
[45] M. A. Langell, C. W. Hutchings, G. A. Carson, and M. H. Nassir, J. Vac. Sci. Technol. A **14**, 1656 (1996).
[46] V. Bayer, C. Franchini, and R. Podloucky, Phys. Rev. B **75**, 035404 (2007).
[47] H. Steininger, S. Lehwald, and H. Ibach, Surf. Sci. **123**, 1 (1982).
[48] B. Fromme, M. Möller, C. Bethke, U. Brunokowski, and E. Kisker, Phys. Rev. B **57**, 12069 (1998).
[49] B. Morosin, Phys. Rev. B **1**, 236 (1970).
[50] F. Bechstedt, *Principles of Surface Physics* (Springer-Verlag, Berlin, 2003).
[51] P. A. Thiry, J. Ghijsen, R. Sporken, J. J. Pireaux, R. L. Johnson, and R. Caudano, Phys. Rev. B **39**, 3620 (1989).
[52] W. Gao, Y. Fujikawa, K. Saiki, and A. Koma, Solid State Commun. **87**, 1013 (1993).
[53] G. T. Tyuliev and K. L. Kostov, Phys. Rev. B **60**, 2900 (1999).
[54] P. A. Thiry, M. Liehr, J. J. Pireaux, and R. Caudano, Phys. Scr. **35**, 368 (1987).
[55] A. A. Lucas, J. P. Vigneron, P. Lambin, P. A. Thiry, M. Liehr, J. J. Pireaux, and R. Caudano, Int. J. Quantum Chem., Quantum Chem. Symp. **19**, 687 (1986).
[56] J. H. Weaver, Phys. Rev. B **11**, 1416 (1975).
[57] A. Seignac and S. Robin, Solid State Commun. **11**, 217 (1972).
[58] K. L. Kostov, P. Jakob, and D. Menzel, Surf. Sci. **377-379**, 802 (1997).